



Precise and versatile microplate reader-based analyses of biosensor signals from arrayed microbial colonies

Hartmann, Fabian S. F.; Weiß, Tamara; Kastberg, Louise L. B.; Workman, Christopher T.; Seibold, Gerd M.

Published in:
Frontiers in Microbiology

Link to article, DOI:
[10.3389/fmicb.2023.1187228](https://doi.org/10.3389/fmicb.2023.1187228)

Publication date:
2023

Document Version
Publisher's PDF, also known as Version of record

[Link back to DTU Orbit](#)

Citation (APA):
Hartmann, F. S. F., Weiß, T., Kastberg, L. L. B., Workman, C. T., & Seibold, G. M. (2023). Precise and versatile microplate reader-based analyses of biosensor signals from arrayed microbial colonies. *Frontiers in Microbiology*, 14, Article 1187228. <https://doi.org/10.3389/fmicb.2023.1187228>

General rights

Copyright and moral rights for the publications made accessible in the public portal are retained by the authors and/or other copyright owners and it is a condition of accessing publications that users recognise and abide by the legal requirements associated with these rights.

- Users may download and print one copy of any publication from the public portal for the purpose of private study or research.
- You may not further distribute the material or use it for any profit-making activity or commercial gain
- You may freely distribute the URL identifying the publication in the public portal

If you believe that this document breaches copyright please contact us providing details, and we will remove access to the work immediately and investigate your claim.



OPEN ACCESS

EDITED BY

Jimmy Tsang,
Shenzhen University, China

REVIEWED BY

Xianjun Chen,
East China University of Science and
Technology, China
Xian Xiao,
Westlake University, China

*CORRESPONDENCE

Gerd M. Seibold
✉ gesei@dtu.dk

[†]These authors have contributed equally to this work and share first authorship

RECEIVED 15 March 2023

ACCEPTED 23 May 2023

PUBLISHED 14 June 2023

CITATION

Hartmann FSF, Weiß T, Kastberg LLB,
Workman CT and Seibold GM (2023) Precise
and versatile microplate reader-based analyses
of biosensor signals from arrayed microbial
colonies.

Front. Microbiol. 14:1187228.

doi: 10.3389/fmicb.2023.1187228

COPYRIGHT

© 2023 Hartmann, Weiß, Kastberg, Workman
and Seibold. This is an open-access article
distributed under the terms of the [Creative
Commons Attribution License \(CC BY\)](#). The
use, distribution or reproduction in other
forums is permitted, provided the original
author(s) and the copyright owner(s) are
credited and that the original publication in this
journal is cited, in accordance with accepted
academic practice. No use, distribution or
reproduction is permitted which does not
comply with these terms.

Precise and versatile microplate reader-based analyses of biosensor signals from arrayed microbial colonies

Fabian S. F. Hartmann[†], Tamara Weiß[†], Louise L. B. Kastberg,
Christopher T. Workman and Gerd M. Seibold*

Section for Synthetic Biology, Department Bioengineering, Technical University of Denmark (DTU),
Lyngby, Denmark

Genetically encoded fluorescent biosensors have emerged as a powerful tool to support phenotypic screenings of microbes. Optical analyses of fluorescent sensor signals from colonies grown on solid media can be challenging as imaging devices need to be equipped with appropriate filters matching the properties of fluorescent biosensors. Toward versatile fluorescence analyses of different types of biosensor signals derived from arrayed colonies, we investigate here the use of monochromator equipped microplate readers as an alternative to imaging approaches. Indeed, for analyses of the LacI-controlled expression of the reporter mCherry in *Corynebacterium glutamicum*, or promoter activity using GFP as reporter in *Saccharomyces cerevisiae*, an improved sensitivity and dynamic range was observed for a microplate reader-based analyses compared to their analyses via imaging. The microplate reader allowed us to capture signals of ratiometric fluorescent reporter proteins (FRPs) with a high sensitivity and thereby to further improve the analysis of internal pH via the pH-sensitive FRP mCherryEA in *Escherichia coli* colonies. Applicability of this novel technique was further demonstrated by assessing redox states in *C. glutamicum* colonies using the FRP Mrx1-roGFP2. By the use of a microplate reader, oxidative redox shifts were measured in a mutant strain lacking the non-enzymatic antioxidant mycothiol (MSH), indicating its major role for maintaining a reduced redox state also in colonies on agar plates. Taken together, analyses of biosensor signals from microbial colonies using a microplate reader allows comprehensive phenotypic screenings and thus facilitates further development of new strains for metabolic engineering and systems biology.

KEYWORDS

Mrx1-roGFP2, mCherry, GFP, arrayed microbial colonies, genetically encoded biosensors, *Corynebacterium glutamicum*, *Saccharomyces cerevisiae*, *Escherichia coli*

1. Introduction

Phenotypic screening of microbial strain libraries for interesting genetic variants underlies many current investigations ranging from analyses of gene functions in basic research on microbial physiology to high-throughput genetic engineering of tailor-made biotechnological platform organisms (Nichols et al., 2011; Liu and Jiang, 2015; French et al., 2018; Zeng et al., 2020). In the best case scenario the trait of interest is directly

coupled to a phenotypic output such as growth and/or formation of a natural chromophore or fluorophore (Tanaka et al., 2008) allowing the easy identification of the strains of interest (Peters et al., 2016). However, target phenotypes often cannot easily be detected and laborious analytical methods such as HPLC-analyses of metabolite levels would be required to identify interesting candidates. In these cases, genetically encoded biosensors have emerged as a valuable tool to facilitate high-throughput screenings. Such biosensors provide the advantage that an intracellular signal is transduced into an output signal, which can easily be measured from each strain of a library in a high-throughput manner (Kaczmarek and Prather, 2021; Hartmann et al., 2022c).

Organisms possess a variety of mechanisms based on different sensors to monitor and react to the intra- or extracellular accumulation of small molecules, ions, or changes in physical parameters. The properties of these natural sensors can be harnessed by applying synthetic biology tools to develop biosensors for high-throughput screenings (Schallmey et al., 2014). By this means in the widely used transcription factor-based biosensors (TFBs), a transcription factor upon interacting with its effector molecule controls the expression of an actuator gene, e.g., for a fluorescent protein (Mahr and Frunzke, 2016; Ding et al., 2021). Unlike TFBs, fluorescent reporter proteins (FRPs) act as both as sensor and actuator. FRPs undergo conformational changes upon interaction with a target metabolite or a change in physiological state, which is subsequently accompanied by a change in their intrinsic fluorescence characteristics (Bermejo et al., 2011; Martynov et al., 2018). To date, many different TFBs and FRPs are available to measure a broad range of internal metabolites or physiological states in microbial cells (Bermejo et al., 2011; Martinez et al., 2012; Goldbeck et al., 2018; Martynov et al., 2018; Depaoli et al., 2019; Hartmann et al., 2020, 2022a).

Besides the selection of specific biosensors for the screening of strain libraries, the experimental set-up also represents a major determinant to be considered for an efficient screening method. High-throughput analysis of microbial libraries can be conducted in well-plates, on agar plates, via fluorescence-activated cell sorting (FACS), or droplet-based screening (Kaczmarek and Prather, 2021). Compared to FACS or droplet-based screening approaches, screenings conducted in well-plates and on agar plates significantly lowers the throughput that can be achieved. However, it provides the advantage that biosensor signals from tested strain can be directly compared under various conditions (Aguiar-Cervera et al., 2021). Agar plate screens are considered as less laborious and provide a slightly higher throughput when compared to well-plate screens, as incubation capacities for agar plates can be easily scaled to the desired size of the strain library. However, agar plate screenings are dependent on optical readouts

using camera-based imaging systems (Kaczmarek and Prather, 2021). As supplier-specific filters for excitation and emission are required, the flexibility for assessing different fluorescent signals is low (Kaczmarek and Prather, 2021). Furthermore, the fixed position of light sources and camera in the imaging system affects sensitivity and might cause shadow-effects dependent of the location of the colony on the agar plate (Daniel and Lawless, 2017). In contrast, multimode plate readers equipped with monochromators and photomultipliers, commonly applied for well-plate screenings, offer a high flexibility, sensitivity, and easy adaptation of reader properties to the respective biosensor applied.

Despite the aforementioned challenges, we successfully applied the ratiometric FRP mCherryEA biosensor to visualize the internal pH of *E. coli* colonies growing on agar plates measured by a FUSION FX (Vilber) imaging system (Hartmann et al., 2022c). To adequately capture the ratiometric biosensor signals, the imaging system was equipped with two capsules (excitation laser and filter module) for excitation (530 and 440 nm) and a filter for capturing the emission (595 nm) of the pH-sensitive mCherry variant mCherryEA (Hartmann et al., 2022c).

The visualization of other biosensor signals (i.e., the redox biosensor protein Mrx1-roGFP2 with an excitation at 380 nm and 470 nm and an emission at 510 nm (Hartmann et al., 2020)) requires that the imaging system set-up is adapted to the properties of the applied fluorescent protein. Thus, applying another fluorescent protein is not readily possible if such appropriate filter modules are not available. This limitation also extends to most of the widely applied imaging systems for microbial colonies, as most cannot be equipped with varying and/or multiple fluorescence filter modules, and thus cannot be used to capture ratiometric fluorescence signals.

Recently, a standard microplate reader was applied as a tool for image-based real-time gene expression analysis using TFBs in living cells growing on the surface of solid media (Hennessy et al., 2017). By scanning the surface of rectangular OmniTray plates, fluorescence signals from organisms growing on agar allowed for imaging with different resolutions (highest resolution = 360 × 240) (Hennessy et al., 2017). During phenotypic screenings on agar plates, strains are typically pinned from a 96-well source plate as an array of 96, 384, or 1536 colonies on rectangular OmniTray plates (Aguiar-Cervera et al., 2021). Therefore, the positions of the arrayed colonies on the agar plates are identical to the typical array of wells on conventional microplates with ANSI/SLAS footprint specifications used in microplate readers. This prompted us to test standard microplate reader systems for their applicability to assess fluorescence signals from arrayed colonies on agar plates.

In this study we demonstrate the wide applicability of microplate reader-based system to measure fluorescence signals from arrayed colonies on rectangular OmniTray agar plates. This method is shown for different types of biosensors including a TFB based on LacI for regulated mCherry expression in *C. glutamicum*, promoter-based biosensors using yeast enhanced GFP (yeGFP) as fluorescent reporter in *S. cerevisiae*, and the FRP mCherryEA to assess the internal pH in *E. coli* colonies. We further show that the method developed here enables the accurate measurement of redox states for *C. glutamicum* colonies via the ratiometric sensor protein Mrx1-roGFP2 on agar plates.

Abbreviations: CTAB, Cetyltrimethylammonium bromide; DTT, Dithiothreitol; EV, Empty vector; FRP, Fluorescent reporter protein; GFP, Green fluorescent protein; IPTG, Isopropyl β-d-1-thiogalactopyranoside; OD, Optical density; OxD, Oxidation degree; RBS, Ribosomal binding site; RFLU, Relative fluorescence units; roGFP2, Redox sensitive GFP2; TFB, Transcription factor-based biosensor; WT, Wild type.

2. Results and discussion

2.1. Microplate reader-based analysis of transcription factor-based biosensors in *Corynebacterium glutamicum* colonies on agar plates

TFBs are widely used in microbial physiology, metabolic engineering, and synthetic biology. Many designs for TFBs include fluorescent proteins as a reporter, which provides an easy optical readout to screen for high or low fluorescent variants from a library. Genome wide screens are often conducted via arrayed colonies on agar plates, as this approach offers a higher capacity than well-plate based screens and the comparison of different conditions (Kaczmarek and Prather, 2021). However, as stated above, analyses of fluorescence signals from colonies via imaging can be challenging (Göttert et al., 2018).

To compare fluorescence imaging with microplate reader-based measurements, two model strains, *C. glutamicum* (pEKEx2_low-mCherry) and *C. glutamicum* (pEKEx2_high-mCherry), were constructed. The two strains were transformed using plasmids pEKEx2_low-mCherry and pEKEx2_high-mCherry, both consisting of the IPTG inducible promoter P_{tac} but differed in the strength of the ribosomal binding site (RBS) for expression of the reporter mCherry (Figure 1A). To verify the different expression levels, *C. glutamicum* (pEKEx2_low-mCherry) and *C. glutamicum* (pEKEx2_high-mCherry) were cultivated in BHI liquid medium supplemented with different IPTG concentrations followed by endpoint fluorescence analysis using a microplate reader (SpectraMax). As depicted in Figure 1B, both strains revealed an IPTG dose-dependent increase of the respective fluorescence intensity. As expected, the use of a stronger RBS in *C. glutamicum* (pEKEx2_high-mCherry) resulted in a higher maximal mCherry fluorescence level when compared to *C. glutamicum* (pEKEx2_low-mCherry). Moreover, no increased fluorescence levels were measured for the control strain *C. glutamicum* (pEKEx2) with an empty vector (Figure 1B). Analysis of fluorescence levels obtained under fully induced conditions ($> 500 \mu\text{M}$) revealed that fluorescence signals of all three strains were significantly different to each other. In

presence of the highest tested IPTG concentration (5 mM IPTG), fluorescence intensities derived from the high-mCherry construct and the low-mCherry construct were approximately 50-fold and 5-fold higher when compared to the empty vector control, respectively (Figure 1B). The results show that the constructed TFBs possess significantly different mCherry levels and both can clearly be distinguished from background fluorescence levels in liquid cultures using a microplate reader.

To analyze the fluorescence signals derived from colonies of the three test strains *C. glutamicum* (pEKEx2), *C. glutamicum* (pEKEx2_low-mCherry), and *C. glutamicum* (pEKEx2_high-mCherry) via imaging, the strains were spotted on rectangular OmniTray (Singer Instruments, United Kingdom) agar plates supplemented with different IPTG concentrations (0–5 mM). After 48 h of incubation, the mCherry fluorescence was analyzed in a fluorescence filter equipped FUSION FX (Vilber) imaging system. In presence of 5 mM IPTG, colonies carrying the reporter pEKEx2_high-mCherry revealed significantly higher fluorescence intensities (mean value $8.10 \times 10^2 \pm 49$ RFLU) when compared to colonies carrying the empty vector control ($5.11 \times 10^2 \pm 43$ RFLU) (Figures 2A,B). In contrast, statistical analysis via ANOVA revealed that fluorescence signals derived from colonies of *C. glutamicum* (pEKEx2_low-mCherry) ($4.92 \times 10^2 \pm 24$ RFLU) are not significantly different when compared to the empty vector control (Figure 2B). To note, increased exposure times (increased from 800 ms to 1000 ms) resulted in higher fluorescence levels for both the empty vector strain, the low-mCherry as well as high-mCherry variant (Supplementary Figure S1). Albeit, fluorescence signals obtained from the high-mCherry variant reached saturation at exposure times above 800 ms, the signals detected for the low-mCherry variant were still indistinguishable from signals obtained from the empty vector control strains under fully induced conditions (Supplementary Figure S1). Significant differences in the visual detection of biosensor fluorescence are a prerequisite toward rational decision-making during screens and the selection of variants. Thus, imaging is unlikely to be suitable for all biosensors and libraries (Kaczmarek and Prather, 2021).

The accurate positioning of 96-arrayed colonies on rectangular agar plates (in a 96-well scheme) was used to measure each colony

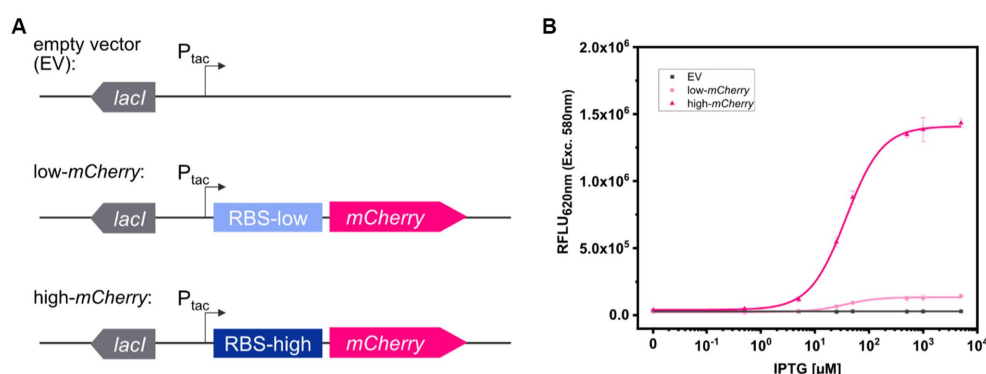


FIGURE 1

Schematic illustration of the genetic constructs for the expression platforms in pEKEx2 with different levels of mCherry translation initiation (A). Relative fluorescence units (RFLU) in presence of different IPTG concentrations after over-night cultivations in liquid media for *C. glutamicum* (pEKEx2) (EV: grey squares), *C. glutamicum* (pEKEx2_low-mCherry) (low-mCherry: light pink circles) and *C. glutamicum* (pEKEx2_high-mCherry) (high-mCherry: dark pink triangles) (B). A Hill function was fit to low-mCherry and high-mCherry data, and a linear fit was used for the empty vector (EV). Error bars represent standard deviation of four biological replicates.

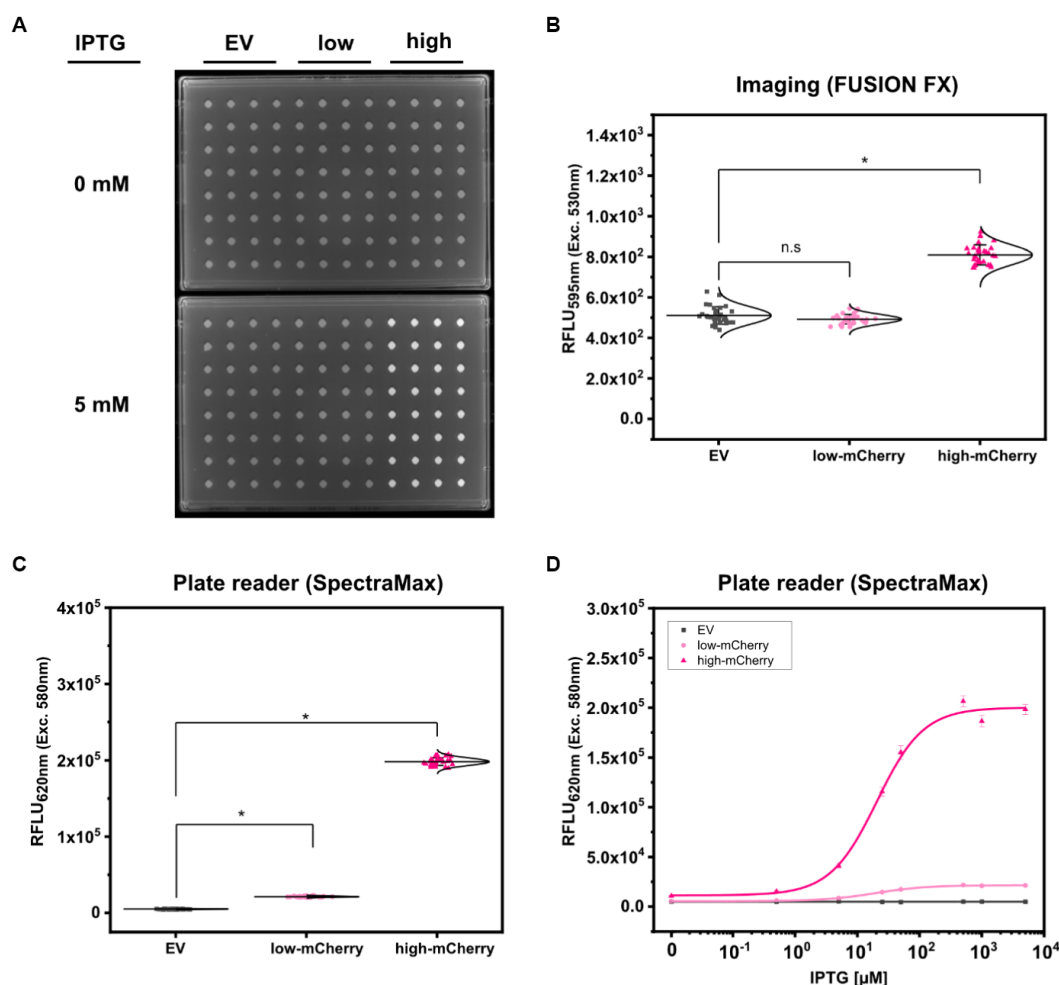


FIGURE 2

Comparison of fluorescence detection of arrayed bacterial colonies on agar plates via imaging and plate reader-based analysis. Representative fluorescence image of 32 colonies of *C. glutamicum* WT (pEKEx2) (EV: grey squares), *C. glutamicum* WT (pEKEx2_low_mCherry) (low-mCherry: light pink circles) and *C. glutamicum* WT (pEKEx2_high_mCherry) (high-mCherry: dark pink triangles) in absence (0mM) or presence (5mM) of IPTG (A), the respective relative fluorescence units (RFLU) for the different colonies (B) and the RFLU values of *C. glutamicum* colonies recorded via a plate reader [SpectraMax iD3 multi-mode plate reader (Molecular Devices LLC, U.S.A)] (C). RFLU values determined for arrayed colonies of EV, low-mCherry and high-mCherry cultivated in presence of different IPTG concentrations (D). For sigmoidal curve fitting, Hill's equation (low-mCherry and high-mCherry) was used. For the EV strain, a linear fit was used. For fluorescence analysis using the plate reader excitation and emission were set to 580 and 620nm, respectively. Imaging of arrayed colonies on agar plates was conducted using the imaging system FUSION FX (Vilber) equipped with a capsule for excitation (530nm) and an emission filter (595nm). Fluorescence signals were statistically analyzed with one-way-ANOVA followed by Tukey's test (n^s $p > 0.05$; $*p \leq 0.001$). Error bars represent standard deviation of 32 colonies.

with the optics of the plate reader. To confirm the accurate positioning of arrayed colonies, we performed an absorbance scan in a 96-well scheme with 30×30 scans per well for an OmniTray agar plate with 96- arrayed colonies in the plate reader (Supplementary Figure S2). The absorbance scan revealed that each colony, corresponding to the respective well, was centered irrespectively of the position of the individually measured colony (Supplementary Figure S2). The exact match of the positioning allowed the plate reader to perform single point measurements similar to measurements performed using 96-well plates. Accordingly, time required for analyses of the 96-colonies can be reduced from 90 min (scan mode) to 20 s (endpoint mode). Thus, the signals obtained from the colonies represent an average value from the colony rather than capturing heterogeneity across the colony.

Based on the precision and accuracy of the colony positions, the same agar plates used for fluorescence imaging were now analyzed using a standard microplate reader. Fluorescence analysis revealed that signals detected via the plate reader for colonies equipped with the high-mCherry construct (average fluorescence of $1.98 \times 10^5 \pm 5.01 \times 10^3$ RFLU), as well as for colonies with the low-mCherry construct ($2.13 \times 10^4 \pm 7.34 \times 10^2$ RFLU), were significantly different when compared to the empty vector control ($4.96 \times 10^3 \pm 2.88 \times 10^2$ RFLU) (Figure 2C).

In addition, we tested the dose-dependent response of the TFB carrying strains *C. glutamicum* (pEKEx2_low_mCherry) and *C. glutamicum* (pEKEx2_high_mCherry) on agar plates with a series of different IPTG concentrations (0–5 mM IPTG; Figure 2D). Hereby, similar dose-response curves were obtained for all strains when

compared to the liquid cultures (Figure 1B). As expected, no IPTG dependent increase of mCherry fluorescence was detected for colonies of the empty vector control strain *C. glutamicum* (pEKEx2). These results demonstrate that a microplate reader can be used for assessing fluorescence signals in arrayed colonies.

2.2. Microplate reader-based system for improved fluorescence analysis of promoter-based biosensors in *Saccharomyces cerevisiae* colonies on agar plates

We next addressed the applicability of the microplate reader-based method for the analysis of fluorescence signals from the broadly used fluorescent protein GFP in colonies of the well-known model-organism *S. cerevisiae*. For this purpose, two model strains of the haploid prototrophic yeast *S. cerevisiae* CEN.PK113-7D (Entian and Kötter, 2007) were constructed by integration of expression cassettes with yeGFP as optical readout. Toward the development of reporter systems with different expression levels, a well-characterized weak constitutive promoter (PDA1) and strong glycolytic promoter (TDH3) were used to control varying levels of yeGFP production (Peng et al., 2015). Prior to analyzing the fluorescence signals from *S. cerevisiae* (background control), *S. cerevisiae* (PDA1-yeGFP) (weak promoter), and *S. cerevisiae* (TDH3p-yeGFP) (strong promoter), strains were arrayed on OmniTray agar plates.

First, fluorescence analyses of GFP signals from arrayed *S. cerevisiae* colonies was performed using the microbial colony CCD imaging workstation Phenobooth (Singer Instruments), equipped with the manufacturer's filters for GFP fluorescence. As depicted in Figure 3A, all colonies of *S. cerevisiae* (background) and *S. cerevisiae* (PDA1-yeGFP) (weak promoter) revealed fluorescence intensities at the same level. In contrast, significantly increased mean fluorescence intensities (1.28 ± 0.14 fold) were measured for colonies of *S. cerevisiae* (TDH3p-yeGFP) (strong promoter). However, individual signals from colonies equipped with the strong promoter still partly overlap with the values derived from the background control colonies. This means that during a random screen a high number of "GFP positive" strains would have remained undetected resulting in a low screening efficiency. Next, fluorescence signals were analyzed by the use of the imaging system FUSION FX (Vilber), equipped with a capsule and a filter for excitation at 435 nm and emission at 480 nm, respectively. The mean fluorescence signals derived from 96 colonies of *S. cerevisiae* (PDA1-yeGFP) (weak promoter) and *S. cerevisiae* (TDH3p-yeGFP) (strong promoter) were significantly increased by 1.30 ± 0.10 fold and 2.37 ± 0.22 fold when compared to the background control, respectively (Figure 3B). Even though not all individual colonies of *S. cerevisiae* (PDA1-yeGFP) can explicitly be distinguished from colonies of the control *S. cerevisiae* strain, which shows background levels of fluorescence, fluorescence analysis via the FUSION FX imaging system has significantly been improved when compared to the use of an imaging workstation (Phenobooth, Singer Instruments).

As a next step, the microplate reader-based method was used to analyze yeGFP signals derived from the different promoters in *S. cerevisiae*. As described for mCherry signals in *C. glutamicum* by

the use of the microplate reader SpectraMax, an average value of $6.62 \times 10^4 \pm 8.59 \times 10^3$ RFLU, $1.19 \times 10^5 \pm 1.22 \times 10^4$ RFLU and $7.46 \times 10^5 \pm 8.74 \times 10^4$ RFLU was determined for *S. cerevisiae* (background), *S. cerevisiae* (PDA1-yeGFP) (weak promoter) and *S. cerevisiae* (TDH3p-yeGFP) (strong promoter), respectively (Figure 3C). This corresponds to a significant 1.80 ± 0.16 fold (weak promoter) and 11.30 ± 1.02 fold (strong promoter) increase when compared to the background control. In contrast to fluorescence imaging, all individual signals obtained for the 96 analyzed colonies harboring both the weak promoter (PDA1-yeGFP) or the strong promoter (TDH3p-yeGFP) possessed higher fluorescence levels when compared to background control colonies (Figure 3C).

To demonstrate transferability of the microplate reader-based approach, we next analyzed fluorescence signals in arrayed colonies using a CLARIOstar^{plus} as a different plate reader device. When compared to *S. cerevisiae*, the mean fluorescence intensity measured for all colonies equipped with the weak promoter (PDA1-yeGFP) and strong promoter (TDH3p-yeGFP) were increased 1.93 ± 0.13 fold and 12.36 ± 0.89 fold, respectively (Figure 3D). These results are in accordance with results obtained via the SpectraMax plate reader.

Taken together, microplate reader-based analysis of colony fluorescence enables the precise and sensitive detection of fluorescence levels of reporter proteins in various microorganisms. To facilitate fluorescence analysis via this approach it is required that the colonies are arrayed in a microtiter-based format. If it is not possible to array the microbial colonies, fluorescence analysis via sensitive imaging systems equipped with adequate sets of filters, such as those used here for the FUSION FX (Vilber) imaging system, are a good alternative, although their incorporation in highly automated workflows is a challenge.

2.3. Microplate reader-based analysis of the pH-sensitive protein mCherryEA improves accuracy of internal pH measurements in *Escherichia coli* colonies

The use of a monochromator equipped microplate reader allowed us to set optimal excitation and emission wavelength settings for the sensitive detection of mCherry and GFP signals from microbial colonies. To test if the versatility and precision of the wavelength settings via the monochromators also enables sensitive analyses of fluorescence signals from ratiometric fluorescent reporter proteins, we aimed to compare analysis of fluorescence signals from the internal pH-sensor protein mCherryEA in arrayed *E. coli* colonies via a plate reader to the recently described approach via fluorescence imaging in a FUSION FX (Vilber) imaging system (Hartmann et al., 2022c).

For this purpose, colonies of the strain *E. coli* MG1655 (pXMJ19_mCherryEA) and the empty vector control strain *E. coli* MG1655 (pXMJ19) were arrayed on SB agar plates (pH 7.0). After cultivation, 5 μ L of PBS buffer supplemented with 0.05% CTAB and with set pH values between 7.0 and 8.5 were applied onto the colonies, as recently described (Hartmann et al., 2022c). At this CTAB concentration the *E. coli* cell membrane is permeabilized allowing the internal pH to become adjusted to the set external pH (Goldbeck et al., 2018). The fluorescence of the colonies was analyzed using an excitation scan (400–590 nm) at an emission wavelength of 630 nm and using the positions of the 96-well

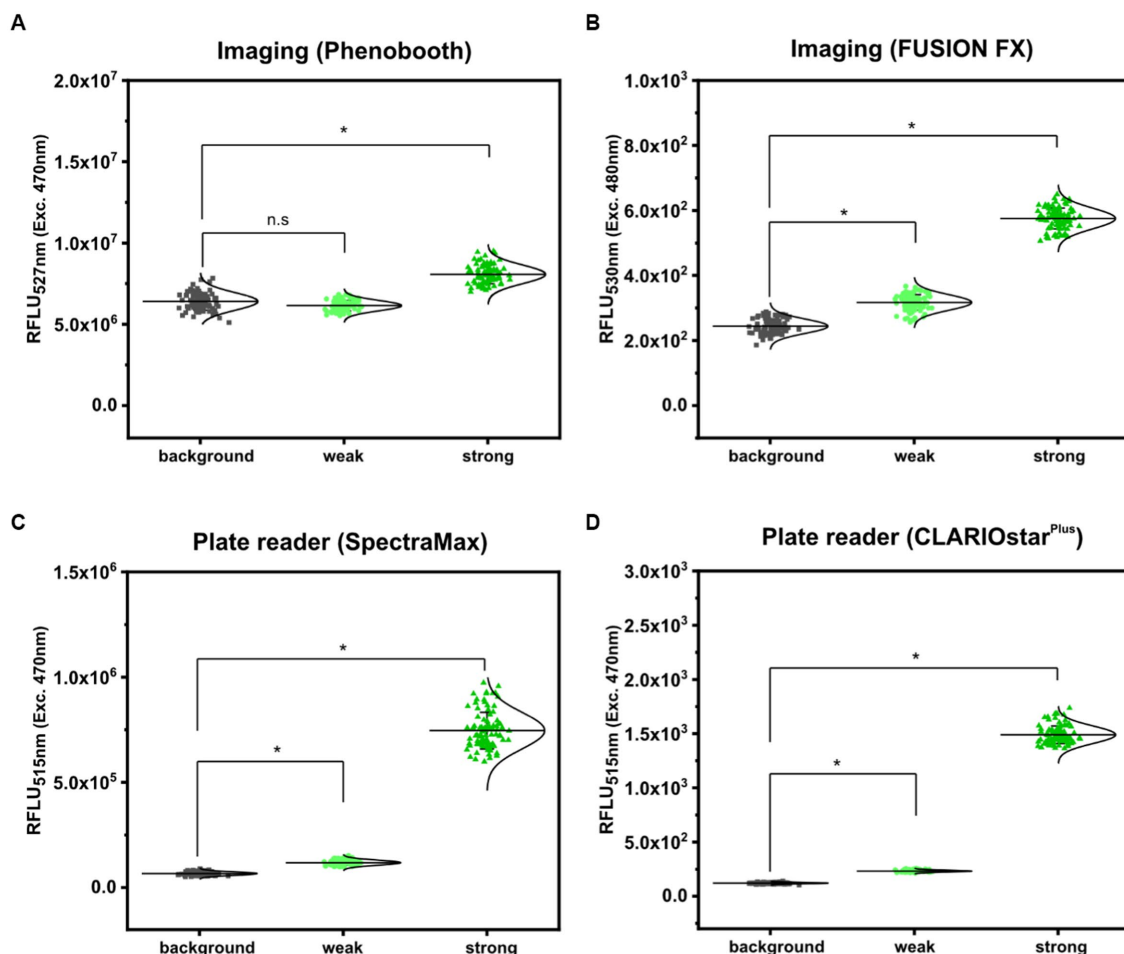


FIGURE 3

Comparison of fluorescence detection of arrayed *Saccharomyces cerevisiae* colonies on agar plates via imaging and plate reader-based analysis. Relative fluorescence units (RFLU) of 96-arrayed colonies of *Saccharomyces cerevisiae* (background; grey squares), *Saccharomyces cerevisiae* (TDH3p-yeGFP) (weak; light green circles) and *Saccharomyces cerevisiae* (PDA1p-yeGFP) (strong, green triangles) analyzed via imaging using the Phenobooth (A) or the FUSION FX (Vilber) (B). Further, fluorescence analysis was performed using the plate reader devices SpectraMax (C) and CLARIOstar^{Plus} (D). RFLU were obtained by normalizing the fluorescence intensity to the colony size (perimeter). Fluorescence signals were statistically analyzed with one-way-ANOVA followed by Tukey's test (^{n.s.} $p > 0.05$; * $p \leq 0.001$). Mean values from 96-replicates are shown (solid horizontal line).

measurement mode of the plate reader. As depicted in Figure 4A, two excitation maxima at 454 nm and 580 nm were obtained for colonies of *E. coli* MG1655 (pXMJ19-*mCherryEA*), which are in accordance to the maxima observed in recently performed excitation scans of bacterial strains harboring the pH-sensitive *mCherryEA* protein in liquid culture (Rajendran et al., 2018; Hartmann et al., 2022c). As expected, no characteristic *mCherryEA* sensor signal was measured for the empty vector control *E. coli* MG1655 (pXMJ19) (Figure 4A). When applying PBS buffer (+ CTAB) with a set pH of 7.0 to the colonies, an emission intensity of 5.8×10^6 FLU was measured at 454 nm excitation, whereas the signal obtained upon an excitation at 580 nm was higher with 6.8×10^6 FLU (Figure 4A); when a PBS buffer (+ CTAB) with a higher pH (8.5) was applied to a colony, the fluorescence intensity obtained for an excitation at 454 nm increased (8.3×10^6 FLU) and decreased at an excitation at 580 nm (4.4×10^6 FLU). This pH-dependent response of the signals for *mCherryEA* at the two excitation wavelengths indicates that the ratiometric response of the biosensor protein *mCherryEA* in *E. coli* colonies on agar plates can

be measured using the microplate reader-based system. Further, fluorescence from *E. coli* MG1655 (pXMJ19-*mCherryEA*) colonies treated with PBS buffer (+ CTAB) with set pH values ranging from 7.0 to 8.5 (Figure 4B) were analyzed using the plate reader (Exc. 454 nm/ 580 nm) and the recently established imaging method (Exc. 440 nm/ Exc. 530 nm) (Hartmann et al., 2022c). The biosensor ratios determined for the imaging method increased linearly from 0.62 ± 0.02 (pH 7.0) to 1.08 ± 0.03 (pH 8.5) upon increasing the pH (Figure 4B). A similar biosensor response was detected with the microplate reader-based method, resulting in an increase from 0.85 ± 0.03 (pH 7.0) to 1.35 ± 0.03 (pH 8.5) (Figure 4B).

Next, 120 colonies arrayed on a rectangular agar plate were analyzed via the two different methods (imaging and plate reader) and the internal pH for each colony determined and visualized with a heat map, where each square corresponds to a single colony (Figure 4C). For both methods, the mean internal pH obtained by the imaging method and the plate reader method was similar with 7.66 ± 0.13 and 7.65 ± 0.03 , respectively (Figure 4D). This agrees with the reported cytoplasmic pH of *E. coli* which is normally

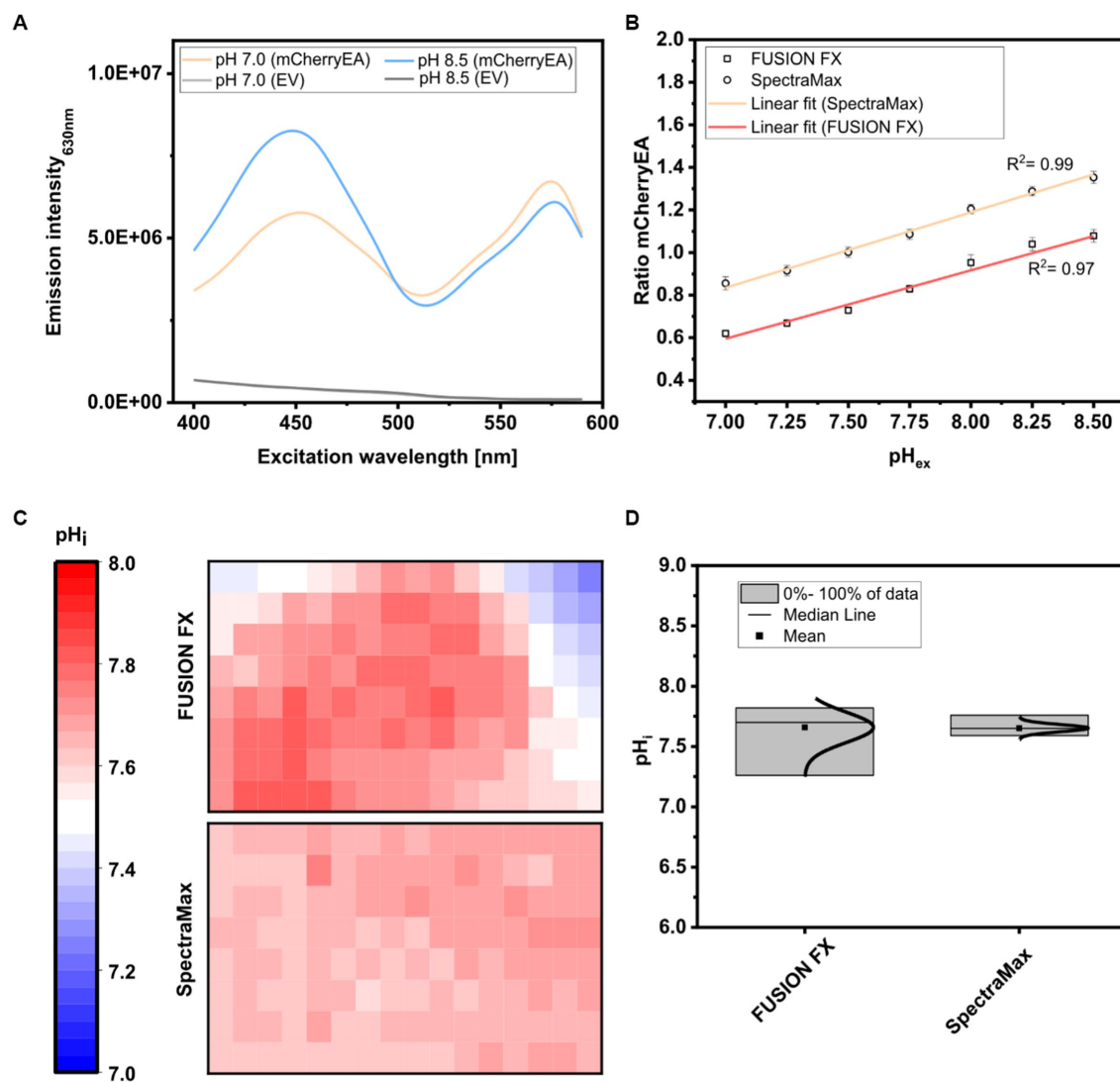


FIGURE 4

Excitation scan (400–590nm) recording the emission intensity at 630nm in colonies of *E. coli* MG1655 (pXMJ19_ mCherryEA) (mCherryEA) and the empty vector control strain *E. coli* MG1655 (pXMJ19) (EV) after applying 5 μ L PBS buffer supplemented with cetyltrimethylammonium bromide [CTAB; final concentration 0.05% (w/v)] with a set pH of 7.0 and 8.5 (A) and ratiometric biosensor signals obtained by dividing the emission intensity at 454nm by 580nm upon applying PBS buffer with pH values ranging from 7.0–8.5 (B). Calculation of the internal pH for biosensor signals recorded from 120 colonies either via imaging using the FUSION FX imaging system equipped with two capsules (Exc. 440nm and Exc. 530nm) and one emission filter (Em. 595nm) as recently described in [Hartmann et al. \(2022c\)](#) or with a microplate reader system (SpectraMax) (C) and data distribution with median and mean values obtained by the two different approaches (D). Error bars represent standard deviation from at least three replicates.

maintained within the range of 7.4–7.9 (Padan et al., 1981; Salmond et al., 1984; Wilks and Slonczewski, 2007) and recently determined internal pH levels in *E. coli* MG1655 colonies on agar plates under similar conditions (Hartmann et al., 2022c). However, differences with respect to the distribution of the determined internal pH values were observed when comparing the data obtained for the two different methods (Figure 4D). The plate reader method established here allowed us to narrow down the distribution from 7.26–7.82 (Δ pH = 0.56; imaging method) to 7.59–7.76 (Δ pH = 0.17; plate reader method), corresponding to a reduction of 0.39 pH units. As the pH is logarithmically and inversely related to the concentrations of hydrogen ions in a solution, the accuracy of the analysis is improved by 390%. The broader distribution obtained by the imaging method might

be caused by reflection artefacts from the transparent edges of the OmniTray plates. To note, the imaging method relies on an one-step excitation of the whole plate, whereas measurements performed in the microplate reader allowed us to measure colonies individually, similar to measurements performed in a 96-well microplate. Moreover, the microplate reader-based method allows operators to set excitation and emission wavelengths on demand and thus perfectly matches the two excitation maxima displayed by the sensor protein mCherryEA. In contrast, the imaging system FUSION FX (Vilber) needs to be equipped with the most suited capsules and filters available (Exc. 440 nm and Exc. 530 nm), which often do not match the properties of the fluorescent protein (Piatkevich et al., 2010; Rajendran et al., 2018; Hartmann et al., 2021).

2.4. Mycothiol is required to maintain a reduced environment in *Corynebacterium glutamicum* colonies growing on agar plates

The improved accuracy using the plate reader-based biosensor analysis represents a significant step forward with respect to screening approaches requiring high sensitivities. Moreover, the high flexibility brought by the monochromatic technology of the plate reader device easily adapts to other fluorescent reporter proteins without causing additional costs and effort to equip imaging devices with appropriate filters. Thus, we next tested this novel technique by applying a ratiometric redox biosensor protein called Mrx1-roGFP2 in *C. glutamicum* colonies.

The abundant low molecular weight (LMW) mycothiol (MSH) functions to maintain the reduced state of the cytoplasm and represents the main non-enzymatic antioxidant in high-GC Gram-positive bacteria, such as the industrial amino acid producer *C. glutamicum* (Liu et al., 2013; Chi et al., 2014; Reyes et al., 2018). Recently, the genetically encoded redox biosensor protein Mrx1-roGFP2 was successfully applied in *C. glutamicum* WT and the MSH-deficient mutant strain *C. glutamicum* $\Delta mshC$ to monitor dynamic redox changes in liquid cultures (Tung et al., 2019; Hartmann et al., 2020). Mutant strains lacking MSH have revealed high susceptibility towards oxidative stress resulting in an impaired growth behavior when cells were exposed to artificial oxidants in shaker-flasks (Chi et al., 2014). In absence of artificial oxidants, growth of the MSH-deficient mutant strain proceeded similar to the wild type strain (Chi et al., 2014; Tung et al., 2019; Hartmann et al., 2020), even though biosensor measurements in the mutant strain revealed an oxidative redox shift (Tung et al., 2019; Hartmann et al., 2020). Detecting intracellular changes (i.e., oxidative stress) prior to the occurrence of a growth defect is an important advance for the development of highly sensitive sensor-based screening approaches. This prompted us to test the analysis of intracellular redox states in arrayed colonies of *C. glutamicum* WT and a mutant strain lacking MSH using the redox biosensor protein Mrx1-roGFP2.

To analyze the redox states in *C. glutamicum* colonies, the 380 nm/470 nm biosensor ratios from 120 arrayed colonies of WT_Mrx1-roGFP2 and the MSH-deficient mutant strain $\Delta mshC$ _Mrx1-roGFP2 were determined. The Mrx1-roGFP2 biosensor consists of redox sensitive GFP2 (roGFP2) which harbors two Cys residues. Upon oxidation it forms a disulfide bond, resulting in an increase of the respective biosensor ratio (Exc. 380 nm/Exc. 470 nm), whereas it responds in the opposite way upon reduction of the biosensor protein. As depicted in Figure 5A, the mean values of the biosensor ratios were significantly different with 0.82 ± 0.01 and 1.52 ± 0.02 for WT_Mrx1-roGFP2 and $\Delta mshC$ _Mrx1-roGFP2, respectively, indicating a more oxidized state of the biosensor protein Mrx1-roGFP2 in the $\Delta mshC$ _Mrx1-roGFP2 strain background on agar plates (Figure 5A). This is in accordance to previous measurements conducted in liquid cultures with biosensor ratios of 1.0 ± 0.02 (WT_Mrx1-roGFP2) and 1.52 ± 0.03 ($\Delta mshC$ _Mrx1-roGFP2) (Hartmann et al., 2020).

Further, we validated the dynamic response and functionality of the sensor protein Mrx1-roGFP2 in colonies by applying Dithiothreitol (DTT; 100 mM) and sodium hypochlorite (NaOCl; 100 mM) as reducing and oxidizing agents, respectively. For this, 5 μ L drops were applied onto WT_Mrx1-roGFP2 and $\Delta mshC$ _Mrx1-roGFP2 colonies followed by real-time monitoring of the biosensor signals. Prior to the colony

treatment, WT_Mrx1-roGFP2 was maintaining stable biosensor ratios between 0.76–0.78 followed by a strong reduction or increase of the biosensor ratio upon applying DTT or NaOCl, respectively (Figure 5B). After 5 min of incubation, fully reduced (DTT; biosensor ratio of 0.53) and fully oxidized (NaOCl; biosensor ratio of 1.4) biosensor ratios were recorded until the end of the experiment (Figure 5B). The treatment with PBS only temporarily induced a slight decrease of the recorded biosensor ratio but then was restored to initially recorded biosensor ratios (Figure 5B). In contrast, $\Delta mshC$ _Mrx1-roGFP2 colonies revealed biosensor ratios between 1.4–1.45 prior to the treatment of the colonies. The addition of DTT buffer solution resulted in a strong reduction of the biosensor ratio reaching fully reduced ratios of 0.54, six to eight min following the treatment (Figure 5C). As expected, treatment with NaOCl just slightly increased the ratio to 1.54 due to its almost fully oxidized state, when compared to a final biosensor ratio of 1.4 for colonies treated with PBS buffer only (Figure 5C). To note, no alteration of the recorded fluorescence signals were observed when performing the same experiment using the *C. glutamicum* WT control strain, indicating that the measured change of the ratiometric biosensor signals in both sensor strains can be attributed to the biosensor protein Mrx1-roGFP2 (Supplementary Figure S3).

Based on the measured biosensor ratios, the oxidation degree (OxD) of the biosensor protein Mrx1-roGFP2 was calculated according to equation 1. OxD values of 0.93 ± 0.03 and 0.33 ± 0.03 were calculated for the Mrx1-roGFP2 biosensor in $\Delta mshC$ _Mrx1-roGFP2 and WT_Mrx1-roGFP2 colonies on agar plates, respectively (Figure 5D). The results are consistent with previous studies performed in shaker-flasks under non-stressed conditions where OxD values between 0.3–0.5 were reported for WT_Mrx1-roGFP2 (Tung et al., 2019; Hartmann et al., 2020). In contrast, almost fully oxidized biosensor states were reported for the MSH-deficient mutant strain (OxD = 0.8–0.95) (Tung et al., 2019; Hartmann et al., 2020). Upon the formation of ROS, the redox-active sulfhydryl group of MSH can either scavenge free radicals directly or functions as a cofactor for antioxidant enzymes resulting in formation of oxidized mycothiol disulfide (MSSM) (Pedre et al., 2015; Si et al., 2015; Tossounian et al., 2015; Si et al., 2016; Reyes et al., 2018). Accordingly, the lack of MSH elevates the intracellular ROS levels and in turn induces an auto-oxidation of the biosensor protein Mrx1-roGFP2 in $\Delta mshC$ _Mrx1-roGFP2. Thus, previous results and the results of this study indicate the major role of MSH for the overall redox homeostasis under aerobic growth conditions in shaker-flask cultivations but also in colonies growing on agar plates.

2.5. Ratiometric biosensor signals are independent of the colony size

Fluorescence signals derived from single fluorescent proteins need to be normalized to the OD₆₀₀ (96-well screen) or colony size (agar screen). In contrast to single fluorescent proteins, a ratiometric fluorescent protein can be normalized to the second fluorescence signal rather than growth related parameters. This implies that a ratiometric biosensor signal should not be affected by changes of the colony size during screens on agar plates.

To test this, a dilution series (different set OD₆₀₀) of *C. glutamicum* WT (WT), *C. glutamicum* WT_Mrx1-roGFP2 (WT_Mrx1-roGFP2) and *C. glutamicum* $\Delta mshC$ _Mrx1-roGFP2 ($\Delta mshC$ _Mrx1-roGFP2) was spotted on rectangular OmniTray plates with solidified CGXII

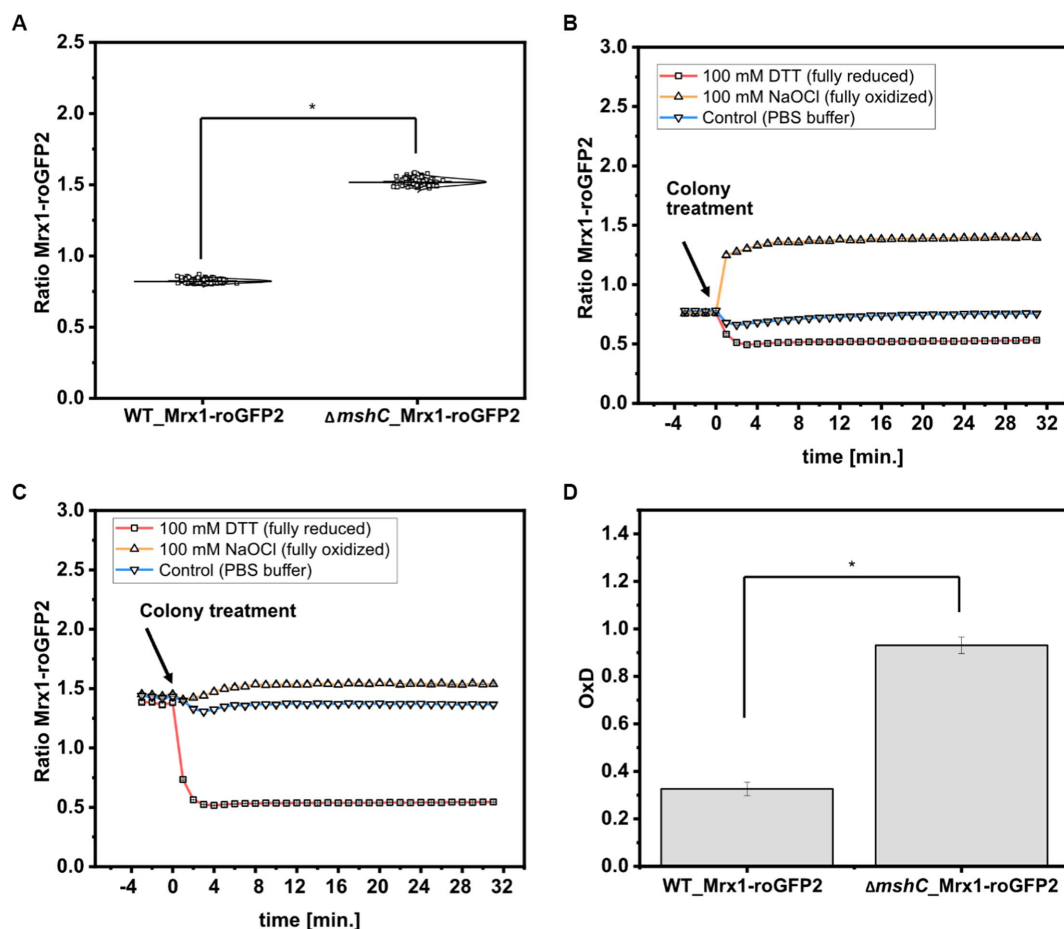


FIGURE 5

Calculated biosensor ratio (Exc. 380nm/ Exc. 470nm) of the sensor protein Mrx1-roGFP2 in colonies of *C. glutamicum* WT_Mrx1-roGFP2 (WT_Mrx1-roGFP2) and *C. glutamicum* $\Delta mshC_Mrx1-roGFP2$ ($\Delta mshC_Mrx1-roGFP2$) (A) and real-time monitoring of the response of the ratiometric signal of the biosensor Mrx1-roGFP2 upon applying DTT (100mM) (reducing agent), hypochlorite (100mM) (oxidizing agent) and PBS buffer (control) onto WT_Mrx1-roGFP2 (B) and $\Delta mshC_Mrx1-roGFP2$ colonies (C). Calculation of the oxidation degree (OxD) by normalizing biosensor ratios to fully oxidized and reduced states (D). For sensor analysis (A,D), 30 colonies from four independent agar plates and experiments were analyzed for each strain (120 colonies in total). Biosensor ratios were analyzed with one-way-ANOVA followed by Tukey's test ($^{**}p > 0.05$; $^{*}p \leq 0.001$). Averaged biosensor ratios from three kinetic experiments are shown (B,C). Error bars are smaller than the size of the symbols used to indicate the biosensor ratios at different time-points.

minimal medium (1% Glucose) (Figure 6A). After 48h of incubation, the final colony size was determined for all spotted dilutions and the size reduction calculated relative to the highest applied OD₆₀₀ (Figure 6A). For the highest applied OD₆₀₀ (10¹), defined as 100% colony size, the area was determined to be 680 ± 29, 610 ± 52 and 590 ± 49 pixels for the WT, WT_Mrx1-roGFP2 and the $\Delta mshC_Mrx1-roGFP2$ colonies, respectively (Figure 6A). Upon applying higher dilutions (stepwise 1:10), the relative colony size was reduced by approximately 10% for each dilution step and a relative colony size of 55 ± 8%, 61 ± 2% and 54 ± 0.4% was reached upon applying an OD₆₀₀ of 10⁻³ for the WT, WT_Mrx1-roGFP2 and $\Delta mshC_Mrx1-roGFP2$ strain, respectively (Figure 6A). For this dilution, the circular morphology of the colonies was impaired leading to inaccuracies with respect to the colony size determination for further dilutions (Figure 6A). Next, the positions of the arrayed colonies from the dilution series were selected and the fluorescence intensity derived from the sensor protein Mrx1-roGFP2 analyzed. Absolute fluorescence intensities measured at 510nm (Exc. 470nm) revealed increased fluorescence levels in colonies of WT_Mrx1-roGFP2 (5.4 ×

10⁶–1.3 × 10⁷ FLU) and $\Delta mshC_Mrx1-roGFP2$ (4.2 × 10⁶–1.03 × 10⁷ FLU) strains when compared to the parental wild type strain *C. glutamicum* (1.90–3.90 × 10⁶ FLU) (Figure 6B). Absolute fluorescence intensities decreased upon a reduction of the colony size (Figure 6B). In accordance with the fluorescence analysis for mCherry or GFP in the previous sections, relative fluorescence intensities were calculated by normalizing the absolute fluorescence intensity to the perimeter of the colony. As expected, fluorescence signals normalized to the measured perimeter of the colonies resulted in stable relative fluorescence intensities until a colony size reduction of 70% was reached (Supplementary Figure S4). Next, the second fluorescence signal (Exc. 380nm/Em. 510nm) was measured for all colonies and the biosensor ratio calculated (Exc. 380nm/ Exc. 470nm). The ratiometric biosensor signal, independently of the colony size, remained stable between 1.0–1.1 and 1.4–1.5 in WT_Mrx1-roGFP2 and $\Delta mshC_Mrx1-roGFP2$ colonies, respectively (Figure 6C). As discussed in the previous section, higher biosensor ratios measured for the MSH-deficient strain are caused by the more oxidized state of the biosensor protein Mrx1-roGFP in this strain

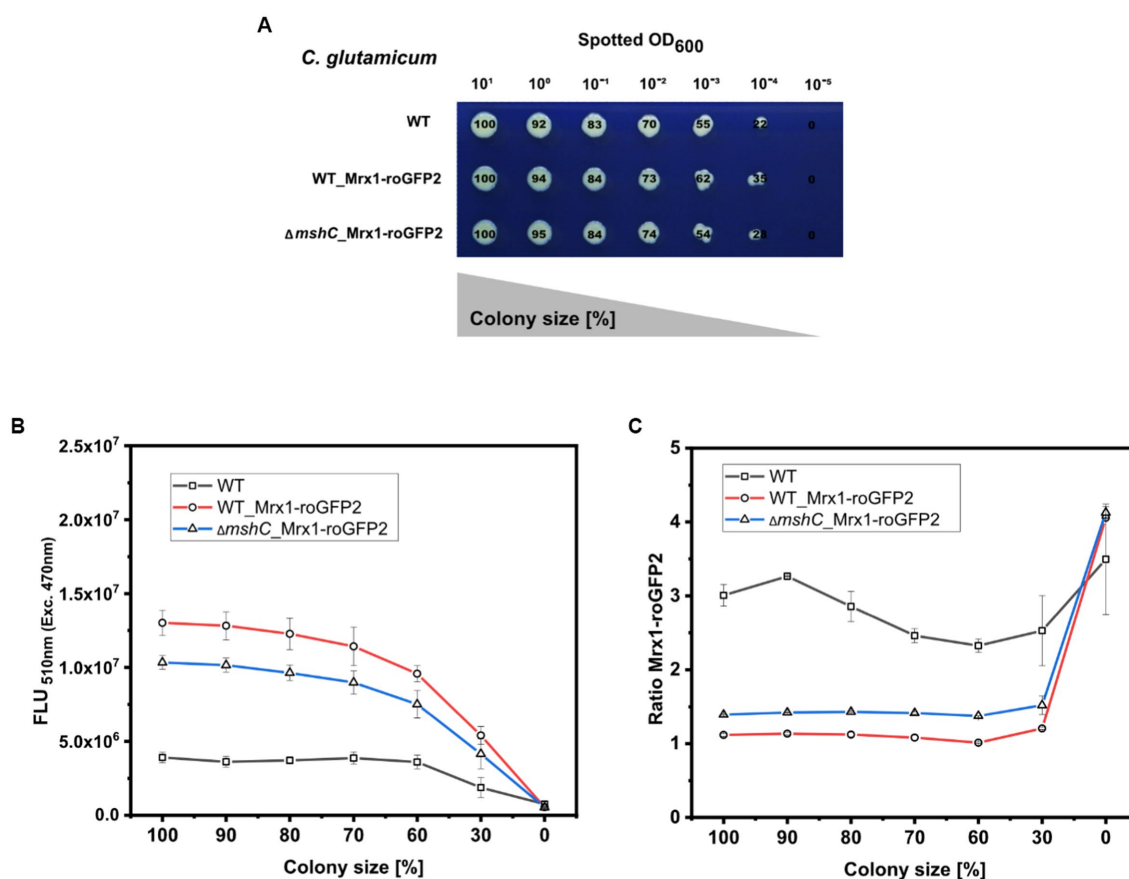


FIGURE 6

Robotic spotting of a dilution series of *C. glutamicum* WT (WT), *C. glutamicum* WT_Mrx1-roGFP2 (WT_Mrx1-roGFP2) and *C. glutamicum* ΔmshC_Mrx1-roGFP2 (ΔmshC_Mrx1-roGFP2) liquid cultures with different set optical densities measured at 600nm (OD₆₀₀) and determination of the colony size relative to the highest spotted OD₆₀₀ (A). Absolute fluorescence intensities measured at 510nm (Exc. 470nm) to validate the presence of Mrx1-roGFP2 in WT_Mrx1-roGFP2 and ΔmshC_Mrx1-roGFP2 colonies (B), and the ratiometric biosensor signal of Mrx1-roGFP2 in the different colonies (C). Robotic spotting was performed using a replica plating Robot ROTOR. Dilution series was grown on OmniTray plates with CGXII media supplemented with 1% Glucose (w/v). Fluorescence analysis of the colonies from the dilution series was performed in a microplate reader (SpectraMax iD3). For the calculation of the ratiometric biosensor signal, the emission intensity at 510nm was recorded upon an excitation at 380nm and 470nm and the former was divided by the latter (Exc. 380nm/Exc. 470nm). Mean values from two independent experiments are shown.

background. To note, increased ratiometric signals (between 2.5 to 4.0) for the agar surface (no colony) and for *C. glutamicum* not harboring the biosensor protein Mrx1-roGFP2 are due to low background fluorescence at 510 nm (Exc. 470 nm) but a higher background fluorescence at 510 nm when excited at 380 nm (Figure 6C).

Taken together, the results demonstrate that the signal derived from a ratiometric biosensor is robust against variations of colony size and the morphology of colonies (Figure 6C). This makes ratiometric FRPs a powerful tool when conducting screens of mutant libraries comprising different phenotypes (e.g., growth behavior). Furthermore, agar plate-based screens provide the advantage that the tested strains can be exposed to various conditions at the same time (replica plating) (Aguiar-Cervera et al., 2021; Navarrete et al., 2022). Conducting screens under industrially relevant conditions (e.g., pH gradients) supported by the use of ratiometric “stress” biosensors will facilitate the development of structured metabolic models for industrially relevant organisms. This bridges metabolic engineering and bioprocess development allowing for the development of computational models suitable for both cell factory design and process optimization at industrial scales in the future (Hartmann et al., 2022b).

3. Conclusion

Phenotypic screenings using arrayed colonies is a widely applied approach to screen strain libraries for particular variants with desired phenotypes. Genetically encoded biosensors are powerful analytical tools to support the rational decision making for strain selection as intracellular states can easily be assessed in a high-throughput manner. However, imaging analysis often limits the applicability of biosensors as the optical set-up of the utilized imaging device does not match with the properties of the fluorescent protein. The microplate reader-based system for sensor analysis established here provides the advantage of a monochromatic technology, which provides high flexibility with respect to different excitation and emission wavelengths. This novel technique has revealed high sensitivity for the detection of low fluorescence levels making it attractive for the development and optimization of genetic circuits regulating harmful targets. In addition, the monochromatic technology enables great opportunities to utilize FRPs, which application to date is often limited due to their complex ratiometric fluorescent properties. The ratiometric readout makes

these types of biosensors highly robust against signal fluctuations caused by the colony size or morphology of the colony. Moreover, applications of such biosensors enable the measurement of complex intracellular states such as oxidative stress or the internal pH in real-time due to their fast dynamics. The microplate reader-based analysis established here can easily be adapted to further biosensors and combinations thereof without causing additional costs and effort to install adequate filter modules. Thus, this technique is expected to provide new possibilities for comprehensive phenotypic screenings and novel applications in metabolic engineering and systems biology.

4. Materials and methods

4.1. Strains, media, and culture conditions

Bacterial strains, yeast strains, and plasmids used in this study are listed in [Table 1](#). Cloning was carried out using *E. coli* DH5 α , cultivated in Lysogeny Broth (LB) medium ([Bertani, 2004](#)). *C. glutamicum* was cultivated using BHI- media (Sigma Aldrich, Germany). *E. coli* MG1655 was cultivated in SB- medium (5 g/L yeast extract; 10 g/L BactoTryptone; 100 mM NaCl; 50 mM KCl, buffered with 50 mM TRIS; pH 7.0) as recently described ([Hartmann et al.,](#)

TABLE 1 Bacterial strains, yeast strains and plasmids used in this study.

Bacterial strains/Plasmids	Description	Reference/Resource
<i>Escherichia coli</i>		
<i>E. coli</i> DH5 α	F- ϕ 80dlacZ Δ (lacZYA-argF) U169 deoRsupE44 Δ lacU169 (f80lacZDM15) hsdR17 recA1 endA1 (rk- mk+) supE44gyrA96 thi-1 gyrA69 relA1	Studier and Moffatt (1986)
<i>E. coli</i> MG1655	F ⁻ lambda- ilvG-rfb-50rpH-1	Blattner et al. (1997)
<i>E. coli</i> MG1655 (pXMJ19)	<i>E. coli</i> MG1655 carrying the vector pXMJ19	Hartmann et al. (2022c)
<i>E. coli</i> MG1655 (pXMJ19_ <i>mCherryEA</i>)	<i>E. coli</i> MG1655 carrying a derivative of pXMJ19 for IPTG-inducible <i>mCherryEA</i> expression	Hartmann et al. (2022c)
<i>Corynebacterium glutamicum</i> ATCC 13032		
<i>C. glutamicum</i> (pEKEx2)	<i>C. glutamicum</i> WT carrying the shuttle vector pEKEx2	This study
<i>C. glutamicum</i> (pEKEx2_low_ <i>mCherry</i>)	<i>C. glutamicum</i> WT carrying a derivative of the shuttle vector pEKEx2 for IPTG inducible expression of the <i>mCherry</i> gene	This study
<i>C. glutamicum</i> (pEKEx2_high_ <i>mCherry</i>)	<i>C. glutamicum</i> WT carrying a derivative of the shuttle vector pEKEx2 for IPTG inducible expression of the <i>mCherry</i> gene	This study
<i>C. glutamicum</i> WT_Mrx1-roGFP2	<i>C. glutamicum</i> WT with integrated <i>P_{trp}-mrx1-roGFP2</i> into the intergenic region of <i>cg1121-cg1122</i>	Tung et al. (2019)
<i>C. glutamicum</i> Δ mshC_Mrx1-roGFP2	<i>C. glutamicum</i> WT deletion of <i>mshC</i> and integrated <i>P_{trp}-mrx1-roGFP2</i> into the intergenic region of <i>cg1121-cg1122</i>	Tung et al. (2019)
<i>Saccharomyces cerevisiae</i> CEN.PK113-7D		
<i>S. cerevisiae</i> (TDH3p-yeGFP_XII-1)	<i>S. cerevisiae</i> with integrated TDH3p-yeGFP-CYC1t and NatMX resistance cassette into the intergenic integration site XII-1	This study
<i>S. cerevisiae</i> (PDA1p-yeGFP_XII-1)	<i>S. cerevisiae</i> with integrated PDA1p-yeGFP-CYC1t and NatMX resistance cassette into the intergenic integration site XII-1	This study
Plasmids		
pEKEx2	Expression vector; <i>ptac lacI^s Km^r</i>	Eikmanns et al. (1991)
pXMJ19	Expression vector; <i>ptac lacI^s Cam^r</i>	Jakoby et al. (1999)
pEKEx2_low_ <i>mCherry</i>	pEKEx2 derivative for IPTG-inducible <i>mCherry</i> gene expression. Upstream of <i>mCherry</i> a weak RBS was inserted.	This study
pEKEx2_high_ <i>mCherry</i>	pEKEx2 derivative for IPTG-inducible <i>mCherry</i> gene expression. Upstream of <i>mCherry</i> a high RBS including a spacer of 6 nt was inserted. This RBS-spacer combination was reported as strong RBS by Shi et al. (2018)	This study
pXMJ19_ <i>mCherryEA</i>	pXMJ19 derivative for IPTG-inducible <i>mCherryEA</i> gene expression	Hartmann et al. (2022c)
pCfB2197	EasyClone system-based yeast integrative vector carrying loxP-flanked natMX marker, integration into <i>S. cerevisiae</i> XII-1 chromosomal location, USER site for cloning amp resistance.	Stovicek et al. (2015)
pLK0106	pCfB2197 containing yeGFP gene under control of PDA1 promoter.	This study
pLK0107	pCfB2197 containing yeGFP gene under control of TDH3 promoter.	This study

2022c). For preparation of agar plates, 16 g/L agar was added to the respective media. Strains carrying plasmids were cultivated in presence of kanamycin (50 µg/mL) or chloramphenicol (20 µg/mL). If required and unless stated otherwise, 1 mM IPTG was added to induce gene expression. The haploid prototrophic yeast *Saccharomyces cerevisiae* strain CEN.PK113-7D was grown in standard yeast peptone dextrose (YPD) medium containing 10 g/L yeast extract, 20 g/L peptone, and 20 g/L glucose and incubated at 30°C. For preparation of YPD agar plates 20 g/L agar was added. For selection of yeast with antibiotic resistance marker NatMX, medium was supplemented with 100 mg/L nourseothricin (ClonNat, Jena Bioscience).

4.2. Strain construction

The two plasmids pEKEx2_low_mCherry and pEKEx2_high_mCherry were assembled via Gibson cloning using the Gibson Assembly® Master Mix (NEB, USA) according to the manufacturer's instructions. For this purpose pEKEx2 was first linearized using SacI (NEB, USA). The gene for mCherry was amplified by PCR using the primer pairs low_mCherry_fw and low_mCherry_rev (Supplementary Table S1) or high_mCherry_fw and high_mCherry_rev for pEKEx2_low_mCherry and pEKEx2_high_mCherry, respectively. All plasmids were introduced into competent *E. coli* DH5α and analyzed via sequencing prior to further use. Transformation of electrocompetent *C. glutamicum* cells and strain validation were performed as described previously (Van der Rest et al., 1999).

To construct the two plasmids pLK0106 and pLK0107 for yeast, DNA fragments constituting the weak PDA1 promoter or the strong TDH3 promoter (Peng et al., 2015) and the yeGFP open reading frame (Cormack et al., 1997) were synthesized as double-stranded gene fragments (Twist Bioscience). The integrative vector pCfB2197 from the EasyClone 2.0 toolkit was used for plasmid construction, which allowed for selection in prototrophic strains (Stovicek et al., 2015). Briefly, the vector was linearized by digestion with *AsiSI* (Life Technologies) restriction endonuclease and nicked with *Nb.BsmI* (New England BioLabs). Synthetic DNA fragments were PCR-amplified - using forward primer FW_USER_TDH3 or FW_USER_PDA1 combined with reverse primer RV_USER_yeGFP - and subsequently cloned into the linearized vector backbone by uracil-excision based (USER) cloning technique (Nour-Eldin et al., 2010; Jensen et al., 2014). Plasmids were transformed into *E. coli* for storage and amplification. Correct plasmid assembly was verified by PCR and Sanger sequencing (Eurofins Genomics) using primers ADH1_test_fw and CYC1_test_rv. Constructed integrative vectors (pLK0106 and pLK0107) were *NotI* (Life Technologies) digested to capture the linear fragments for integration. *S. cerevisiae* was transformed as previously described (Gietz and Schiestl, 2007). For genetic integration of cassettes, 1 µg of linear DNA was transformed into yeast for integration into the XII-1 chromosomal integration site (Mikkelsen et al., 2012). Cells were plated onto selective YPD plates and colonies were re-streaked on selective plates. Genomic DNA was extracted as previously described (Löoke et al., 2011), and integration verified by PCR using XII-1_up and XII-1_down. All oligonucleotides used in this study can be found in the supplementary material (Supplementary Table S1).

4.3. Fluorescence analysis

Fluorescence measurements of liquid cultures were conducted in black clear-bottomed 96-well microplates (Greiner Bio-One, Austria) using a SpectraMax iD3 multi-mode plate reader (Molecular Devices LLC, U.S.A.). For fluorescence analysis of the fluorescent protein mCherry, endpoint measurements were recorded by setting the excitation wavelength at 580 nm and the emission wavelength at 620 nm. For liquid cultures, fluorescence intensities were normalized to the optical density measured at 600 nm (OD₆₀₀) using transparent flat-bottomed 96-well microplates (Greiner bio-one B.V., Netherlands). Prior to measurements of liquid cultures, cells were washed and four times concentrated.

For fluorescence analysis of the pH-sensitive protein mCherryEA, excitation scans were recorded by setting the excitation wavelength between 400 nm and 590 nm and the emission wavelength at 630 nm. For ratiometric analysis of the biosensor signal, the emission maxima obtained upon an excitation at 454 and 580 nm were taken and the corresponding biosensor ratio was calculated by dividing the former emission intensity by the latter as recently described (Hartmann et al., 2022c). For fluorescence analysis of the redox biosensor protein Mrx1-roGFP2, the calculation of Exc. 380 nm/ Exc. 470 nm (Em. 510 nm) was used for the determination of the biosensor ratio as recently described (Hartmann et al., 2020). For determination of the biosensor oxidation degree (OxD), biosensor ratios from untreated samples were normalized to fully reduced (100 mM Dithiothreitol (DTT) in PBS buffer; pH 7.0) or oxidized (100 mM Natriumhypochlorite (NaOCl) in PBS buffer, pH 7.0) samples according to equation 1. Here, $I_{380_{\text{sample}}}$ and $I_{470_{\text{sample}}}$ represent the measured fluorescence intensities received for an excitation at 380 nm and 470 nm, respectively. Fully reduced and oxidized controls are given by $I_{380_{\text{red}}}$, $I_{470_{\text{red}}}$ and $I_{380_{\text{ox}}}$, $I_{470_{\text{ox}}}$, respectively.

$$\text{OxD} = \frac{I_{380_{\text{sample}}} \times I_{470_{\text{red}}} - I_{380_{\text{red}}} \times I_{470_{\text{sample}}}}{I_{380_{\text{sample}}} \times I_{470_{\text{red}}} - I_{380_{\text{sample}}} \times I_{470_{\text{ox}}} + I_{380_{\text{ox}}} \times I_{470_{\text{sample}}} - I_{380_{\text{red}}} \times I_{470_{\text{sample}}}} \quad (1)$$

4.4. Microplate reader-based analysis of sensor signals in colonies on agar plates

Prior to robotic spotting of cell cultures, wells of 96-well microtiter plates (Greiner bio-one B.V., Netherlands) were filled with 200 µL overnight culture adjusted to an OD₆₀₀ of 1 in the respective media. For dilution series, the OD₆₀₀ was set to 10 and 1:10 dilutions prepared in microtiter plates. The working plate (96-well plate) was used as a source plate for robotic spotting using a ROTOR HDA benchtop robot (Singer Instruments, United Kingdom) on rectangular OmniTray plates (Singer Instruments, United Kingdom) with solidified medium on the target plate as recently described⁸. The OmniTray plates were prepared by using 50 mL of the respective media supplemented with appropriate antibiotic and IPTG for biosensor expression if required. Agar plates with spotted cell cultures in an arrayed format were cultivated for 24 h (*E. coli* and *S. cerevisiae* strains) or 48 h for *C. glutamicum* strains if not otherwise stated. Fluorescence analysis was performed using a SpectraMax iD3 multi-mode plate reader (Molecular Devices LLC, U.S.A.). Prior to fluorescence analysis, the lid from the OmniTray plate was removed. A 96-well plate scheme was selected for the measurement mode and the wells selected for targeting

the respective colonies arrayed in a 96-well scheme on the agar plates. Measurement height was set to 5 mm and measurements were performed at ambient temperature.

4.5. Fluorescence imaging of arrayed colonies

Fluorescence imaging of microbial colonies on agar plates was carried out using the photo-documentation system FUSION FX (Vilber Lourmat, France) and the FUSION FX EVOLUTION-CAPT software (Vilber Lourmat) for image analyses. For fluorescence analysis of the fluorescent protein mCherry, the FUSION FX was equipped with a capsule for excitation at 530 nm and an emission filter at 595 nm. For yeGFP analysis a capsule for excitation at 480 nm and a filter for emission 530 nm were used. Exposure time was set to 800 msec if not stated otherwise. Biosensor signals from the pH-sensitive protein mCherryEA were measured using the FUSION FX as recently described⁸. For fluorescence analysis using the Phenobooth (Singer Instruments, United Kingdom), the blue channel was selected for excitation (470 nm) and the emission intensity measured using a GFP filter (527 nm/20 nm).

4.6. Treatment of colonies

To analyze the biosensor response of *E. coli* (pXMJ19_mCherryEA), arrayed colonies were treated using buffers with a different set pH (5 μ L drops), followed by measuring the biosensor response as described above. Similarly, *C. glutamicum* WT_Mrx1-roGFP2 colonies were subjected to buffer drops (5 μ L) supplemented with oxidants (Hypochlorite) or reducing agents (Dithiothreitol) to induce a redox shift in the biosensor. To ensure that the shape and morphology of the colonies were not dispersed, we used a multi-channel pipette to smoothly apply 5 μ L drops of the respective buffer solutions onto the colonies. It is worth noting that the multi-channel pipette can be used to apply drops onto colonies arrayed in both 96 and 384 scheme formats (Mrx1-roGFP2 and mCherryEA, respectively).

4.7. White light imaging and determination of colony sizes

White light images were captured using the Phenobooth (Singer Instruments, United Kingdom). If required, images were processed prior to analyzing the images using Cellprofiler 4 (version 4.0.7) (Stirling et al., 2021). In order to determine colony sizes, the respective images were analyzed via the Python toolbox Pyphe (Kamrad et al., 2020).

4.8. Statistical analysis

Biosensor signals were analyzed using one-way variance (ANOVA) followed by Tukey's test. The respective analysis was performed using Python 3 (Van Rossum and Drake, 2009), and Pandas (McKinney, 2010) was used to handle data frames. ANOVA was performed using the `ols()` and `anova_lm()` function of the `statsmodels` package (Seabold and Perktold, 2010). Tukey's test was performed using `tukey_hsd()` function of the `bioinfokit` package

(Bedre, 2021). Differences were considered significant when value of $p < 0.05$. All data were plotted and visualized using the software Origin.

Data availability statement

The original contributions presented in the study are included in the article/Supplementary material, further inquiries can be directed to the corresponding author.

Author contributions

FH and TW: conceptualization, data curation, formal analysis, investigation, methodology, validation, visualization, writing of original draft, and writing-review and editing. LK: formal analysis, investigation, and writing-review and editing. CW: funding acquisition, and writing-review and editing. GS: conceptualization, funding acquisition, supervision, writing-original draft, and writing-review and editing. All authors contributed to the article and approved the submitted version.

Funding

This work received funding by the Novo Nordisk Fonden within the framework of the Fermentation-based Biomanufacturing Initiative (FBM) (FBM-grant: NNF17SA0031362) and from the Bio Based Industries Joint Undertaking under the European Union's Horizon 2020 research and innovation program (Grant agreement No. 790507).

Acknowledgments

We would like to thank the Fermentation Core at DTU Bioengineering for excellent technical support.

Conflict of interest

The authors declare that the research was conducted in the absence of any commercial or financial relationships that could be construed as a potential conflict of interest.

Publisher's note

All claims expressed in this article are solely those of the authors and do not necessarily represent those of their affiliated organizations, or those of the publisher, the editors and the reviewers. Any product that may be evaluated in this article, or claim that may be made by its manufacturer, is not guaranteed or endorsed by the publisher.

Supplementary material

The Supplementary material for this article can be found online at: <https://www.frontiersin.org/articles/10.3389/fmicb.2023.1187228/full#supplementary-material>

References

- Abe, S., Takayama, K. I., and Kinoshita, S. (1967). Taxonomical studies on glutamic acid-producing Bacteria. *J. Gen. Appl. Microbiol.* 13, 279–301. doi: 10.2323/jgam.13.279
- Aguiar-Cervera, J. E., Delneri, D., and Severn, O. (2021). A high-throughput screening method for the discovery of *Saccharomyces* and non-*Saccharomyces* yeasts with potential in the brewing industry. *Eng. Biol.* 5, 72–80. doi: 10.1049/enb2.12013
- Bedre, R. (2021). Reneshbedre/Bioinfokit: bioinformatics data analysis and visualization toolkit. *Zenodo*. doi: 10.5281/zenodo.4422035
- Bermejo, C., Haerizadeh, F., Takanaga, H., Chermak, D., and Frommer, W. B. (2011). Optein sensors for measuring dynamic changes of cytosolic metabolite levels in yeast. *Nat. Protoc.* 6, 1806–1817. doi: 10.1038/nprot.2011.391
- Bertani, G. (2004). Lysogeny at mid-twentieth century: P1, P2, and other experimental systems. *J. Bacteriol.* 186, 595–600. doi: 10.1128/JB.186.3.595-600.2004
- Blattner, F. R., Plunkett, G., Bloch, C. A., Perna, N. T., Burland, V., Riley, M., et al. (1997). The complete genome sequence of *Escherichia coli* K-12. *Science* 277, 1453–1462. doi: 10.1126/science.277.5331.1453
- Chi, B. K., Busche, T., Van Laer, K., Bäsell, K., Becher, D., Clermont, L., et al. (2014). Protein S-mycotohiolation functions as redox-switch and thiol protection mechanism in *Corynebacterium glutamicum* under hypochlorite stress. *Antioxid. Redox Signal.* 20, 589–605. doi: 10.1089/ars.2013.5423
- Cormack, B. P., Bertram, G., Egerton, M., Gow, N. A. R., Falkow, S., and Brown, A. J. P. (1997). Yeast-enhanced green fluorescent protein (yEGFP): a reporter of gene expression in *Candida albicans*. *Microbiology* 143, 303–311. doi: 10.1099/00221287-143-2-303
- Daniel, B., and Lawless, C. (2017). Modelling competition for nutrients between microbial populations growing on a solid agar surface. *bioRxiv*. doi: 10.1101/086835
- Depaoli, M. R., Bischof, H., Eroglu, E., Burgstaller, S., Ramadani-Muja, J., Rauter, T., et al. (2019). Live cell imaging of signaling and metabolic activities. *Pharmacol. Ther.* 202, 98–119. doi: 10.1016/j.pharmthera.2019.06.003
- Ding, N., Zhou, S., and Deng, Y. (2021). Transcription-factor-based biosensor engineering for applications in synthetic biology. *ACS Synth. Biol.* 10, 911–922. doi: 10.1021/acssynbio.0c00252
- Eikmanns, B. J., Kleinertz, E., Liehl, W., and Sahm, H. (1991). A family of *Corynebacterium glutamicum*/*Escherichia coli* expression and promoter probing. *Plasmid* 102, 93–98. doi: 10.1016/0378-1119(91)90545-M
- Entian, K. D., and Kötter, P. (2007). 25 yeast genetic strain and plasmid collections. *Methods Microbiol.* 36, 629–666. doi: 10.1016/S0580-9517(06)36025-4
- French, S., Coutts, B. E., and Brown, E. D. (2018). Open-source high-throughput phenomics of bacterial promoter-reporter strains. *Cell Syst.* 7, 339–346.e3. doi: 10.1016/j.cels.2018.07.004
- Gietz, R. D., and Schiestl, R. H. (2007). High-efficiency yeast transformation using the LiAc/SS carrier DNA/PEG method. *Nat. Protoc.* 2, 31–34. doi: 10.1038/nprot.2007.13
- Goldbeck, O., Eck, A. W., and Seibold, G. M. (2018). Real time monitoring of NADPH concentrations in *Corynebacterium glutamicum* and *Escherichia coli* via the genetically encoded sensor mBFP. *Front. Microbiol.* 9, 1–10. doi: 10.3389/fmicb.2018.02564
- Göttert, H., Mattiazzi Usaj, M., Rosebrock, A. P., and Andrews, B. J. (2018). Reporter-based synthetic genetic array analysis: a functional genomics approach for investigating transcript or protein abundance using fluorescent proteins in *Saccharomyces cerevisiae*. *Methods Mol. Biol.* 1672, 613–629. doi: 10.1007/978-1-4939-7306-4_40
- Hartmann, F. S. F., Anastasiou, I., Weiß, T., Lkhaasuren, T., and Seibold, G. M. (2022a). Combined sensor-based monitoring of Mycothiol redox potential and DNA-damage response in *Corynebacterium glutamicum*. *bioRxiv*. doi: 10.1101/2022.07.25.501298
- Hartmann, F. S. F., Anastasiou, I., Weiß, T., Shen, J., and Seibold, G. M. (2021). Impedance flow cytometry for viability analysis of *Corynebacterium glutamicum*. *J. Microbiol. Methods* 191:106347. doi: 10.1016/j.mimet.2021.106347
- Hartmann, F. S. F., Clermont, L., Tung, Q. N., Antelmann, H., and Seibold, G. M. (2020). The industrial organism *Corynebacterium glutamicum* requires mycothiol as antioxidant to resist against oxidative stress in bioreactor cultivations. *Antioxidants* 9, 1–13. doi: 10.3390/antiox9100969
- Hartmann, F. S. F., Udugama, I. A., Seibold, G. M., Sugiyama, H., and Gernaey, K. V. (2022b). Digital models in biotechnology: towards multi-scale integration and implementation. *Biotechnol. Adv.* 60:108015. doi: 10.1016/j.biotechadv.2022.108015
- Hartmann, F. S. F., Weiß, T., Shen, J., Smahajcsik, D., Savickas, S., and Seibold, G. M. (2022c). Visualizing the pH in *Escherichia coli* colonies via the sensor protein mCherryEA allows high-throughput screening of Mutant Libraries. *mSystems*, 7–e0021922. doi: 10.1128/mSystems.00219-22
- Hennessy, R. C., Stougaard, P., and Olsson, S. (2017). A microplate reader-based system for visualizing transcriptional activity during in vivo microbial interactions in space and time. *Sci. Rep.* 7, 1–6. doi: 10.1038/s41598-017-00296-4
- Jakoby, M., Carole-Estelle, J., Ngoueto-Nkili, J., and Burkovski, A. (1999). Construction and application of new *Corynebacterium glutamicum* vectors. *Biotechnol. Tech.* 13, 437–441. doi: 10.1023/A:1008968419217
- Jensen, N. B., Strucko, T., Kildegaard, K. R., David, F., Maury, J., Mortensen, U. H., et al. (2014). EasyClone: method for iterative chromosomal integration of multiple genes in *Saccharomyces cerevisiae*. *FEMS Yeast Res.* 14, 238–248. doi: 10.1111/1567-1364.12118
- Kaczmarek, J. A., and Prather, K. L. J. (2021). Effective use of biosensors for high-throughput library screening for metabolite production. *J. Ind. Microbiol. Biotechnol.* 48, 9–10. doi: 10.1093/jimb/kuab049
- Kamrad, S., Rodríguez-López, M., Cotobal, C., Correia-Melo, C., Ralser, M., and Bähler, J. (2020). Pyphe, a python toolbox for assessing microbial growth and cell viability in high-throughput colony screens. *elife* 9:9. doi: 10.7554/eLife.55160
- Liu, W., and Jiang, R. (2015). Combinatorial and high-throughput screening approaches for strain engineering. *Appl. Microbiol. Biotechnol.* 99, 2093–2104. doi: 10.1007/s00253-015-6400-0
- Liu, Y. B., Long, M. X., Yin, Y. J., Si, M. R., Zhang, L., Lu, Z. Q., et al. (2013). Physiological roles of mycothiol in detoxification and tolerance to multiple poisonous Chemicals in *Corynebacterium glutamicum*. *Arch. Microbiol.* 195, 419–429. doi: 10.1007/s00203-013-0889-3
- Löoke, M., Kristjuhan, K., and Kristjuhan, A. (2011). Extraction of genomic DNA from yeasts for PCR-based applications. *BioTechniques* 50, 325–328. doi: 10.2144/000113672.EXTRACTION
- Mahr, R., and Frunzke, J. (2016). Transcription factor-based biosensors in biotechnology: current state and future prospects. *Appl. Microbiol. Biotechnol.* 100, 79–90. doi: 10.1007/s00253-015-7090-3
- Martinez, K. A., Kitko, R. D., Mershon, J. P., Adcox, H. E., Malek, K. A., Berkmen, M. B., et al. (2012). Cytoplasmic pH response to acid stress in individual cells of *Escherichia coli* and *Bacillus subtilis* observed by fluorescence ratio imaging microscopy. *Appl. Environ. Microbiol.* 78, 3706–3714. doi: 10.1128/AEM.00354-12
- Martynov, V. I., Pakhomov, A. A., Deyev, I. E., and Petrenko, A. G. (2018). Genetically encoded fluorescent indicators for live cell pH imaging. *Biochim. Biophys. Acta Gen. Subj.* 1862, 2924–2939. doi: 10.1016/j.bbagen.2018.09.013
- McKinney, W. Data structures for statistical computing in Python. In Proceedings of the 9th python in science conference; (2010).
- Mikkelsen, M. D., Buron, L. D., Salomonsen, B., Olsen, C. E., Hansen, B. G., Mortensen, U. H., et al. (2012). Microbial production of indolylglucosinolate through engineering of a multi-gene pathway in a versatile yeast expression platform. *Metab. Eng.* 14, 104–111. doi: 10.1016/j.ymben.2012.01.006
- Navarrete, C., Estrada, M., and Martínez, J. L. (2022). *Debaryomyces hansenii*: an old acquaintance for a fresh start in the era of the green biotechnology. *World J. Microbiol. Biotechnol.* 38, 99–10. doi: 10.1007/s11274-022-03280-x
- Nichols, R. J., Sen, S., Choo, Y. J., Beltrao, P., Zietek, M., Chaba, R., et al. (2011). Phenotypic landscape of a bacterial cell. *Cells* 144, 143–156. doi: 10.1016/j.cell.2010.11.052
- Nour-Eldin, H. H., Geu-Flores, F., and Halkier, B. A. (2010). USER cloning and USER Fusion: the ideal cloning techniques for small and big laboratories. *Methods Mol. Biol.* 643, 185–200. doi: 10.1007/978-1-60761-723-5
- Padan, E., Zilberstein, D., and Schuldiner, S. (1981). pH homeostasis in bacteria. *Biochim. Biophys. Acta* 650, 151–166. doi: 10.1016/0304-4157(81)90004-6
- Pedre, B., Van Molle, I., Villadangos, A. F., Wahni, K., Vertommen, D., Turell, L., et al. (2015). The *Corynebacterium glutamicum* mycothiol peroxidase is a reactive oxygen species-scavenging enzyme that shows promiscuity in thiol redox control. *Mol. Microbiol.* 96, 1176–1191. doi: 10.1111/mmi.12998
- Peng, B., Williams, T. C., Henry, M., Nielsen, L. K., and Vickers, C. E. (2015). Controlling heterologous gene expression in yeast cell factories on different carbon substrates and across the diauxic shift: a comparison of yeast promoter activities. *Microb. Cell Factories* 14, 1–11. doi: 10.1186/s12934-015-0278-5
- Peters, J. M., Colavin, A., Shi, H., Czarny, T. L., Larson, M. H., Wong, S., et al. (2016). A comprehensive, CRISPR-based functional analysis of essential genes in bacteria. *Cells* 165, 1493–1506. doi: 10.1016/j.cell.2016.05.003
- Piatkevich, K. D., Malashkevich, V. N., Almo, S. C., and Verkhusa, V. V. (2010). Engineering ESPT pathways based on structural analysis of LSsmKate red fluorescent proteins with large stokes shift. *J. Am. Chem. Soc.* 132, 10762–10770. doi: 10.1021/ja101974k
- Rajendran, M., Claywell, B., Haynes, E. P., Scales, U., Henning, C. K., and Tantama, M. (2018). Imaging pH dynamics simultaneously in two cellular compartments using a ratiometric pH-sensitive mutant of mCherry. *ACS Omega* 3, 9476–9486. doi: 10.1021/acsomega.8b00655
- Reyes, A. M., Pedre, B., De Armas, M. I., Tossounian, M. A., Radi, R., Messens, J., et al. (2018). Chemistry and redox biology of mycothiol. *Antioxid. Redox Signal.* 28, 487–504. doi: 10.1089/ars.2017.7074
- Salmond, C. V., Kroll, R. G., and Booth, I. R. (1984). The effect of food preservatives on pH homeostasis in *Escherichia coli*. *J. Gen. Microbiol.* 130, 2845–2850. doi: 10.1099/00221287-130-11-2845

- Schallmeyer, M., Frunzke, J., Eggeling, L., and Marienhagen, J. (2014). Looking for the pick of the bunch: high-throughput screening of producing microorganisms with biosensors. *Curr. Opin. Biotechnol.* 26, 148–154. doi: 10.1016/j.copbio.2014.01.005
- Seabold, S., and Perktold, J. Statsmodels: econometric and statistical modeling with Python. In Proceedings of the 9th python in science conference (2010).
- Shi, F., Luan, M., and Li, Y. (2018). Ribosomal binding site sequences and promoters for expressing glutamate decarboxylase and producing γ -aminobutyrate in *Corynebacterium glutamicum*. *AMB Express* 8:61. doi: 10.1186/s13568-018-0595-2
- Si, M., Xu, Y., Wang, T., Long, M., Ding, W., Chen, C., et al. (2015). Functional characterization of a mycothiol peroxidase in *Corynebacterium glutamicum* that uses both mycoredoxin and thioredoxin reducing systems in the response to oxidative stress. *Biochem. J.* 469, 45–57. doi: 10.1042/BJ20141080
- Si, M., Zhao, C., Zhang, B., Wei, D., Chen, K., Yang, X., et al. (2016). Overexpression of mycothiol disulfide reductase enhances *Corynebacterium glutamicum* robustness by modulating cellular redox homeostasis and antioxidant proteins under oxidative stress. *Sci. Rep.* 6, 1–14. doi: 10.1038/srep29491
- Stirling, D. R., Swain-Bowden, M. J., Lucas, A. M., Carpenter, A. E., Cimini, B. A., and Goodman, A. (2021). CellProfiler 4: improvements in speed, utility and usability. *BMC Bioinform.* 22:433. doi: 10.1186/s12859-021-04344-9
- Stovicek, V., Borja, G. M., Forster, J., and Borodina, I. (2015). EasyClone 2.0: expanded toolkit of integrative vectors for stable gene expression in industrial *Saccharomyces cerevisiae* strains. *J. Ind. Microbiol. Biotechnol.* 42, 1519–1531. doi: 10.1007/s10295-015-1684-8
- Studier, F. W., and Moffatt, B. A. (1986). Use of bacteriophage T7 RNA polymerase to direct selective high-level expression of cloned genes. *J. Mol. Biol.* 189, 113–130. doi: 10.1016/0022-2836(86)90385-2
- Tanaka, Y., Sasaki, N., and Ohmiya, A. (2008). Biosynthesis of plant pigments: anthocyanins, betalains and carotenoids. *Plant J.* 54, 733–749. doi: 10.1111/j.1365-3113X.2008.03447.x
- Tossounian, M. A., Pedre, B., Wahn, K., Erdogan, H., Vertommen, D., Van Molle, I., et al. (2015). *Corynebacterium diphtheriae* methionine sulfoxide reductase exploits a unique mycothiol redox relay mechanism. *J. Biol. Chem.* 290, 11365–11375. doi: 10.1074/jbc.M114.632596
- Tung, Q. N., Loi, V., Van Busche, T., Nerlich, A., Mieth, M., Milse, J., et al. (2019). Stable integration of the Mrx1-roGFP2 biosensor to monitor dynamic changes of the mycothiol redox potential in *Corynebacterium glutamicum*. *Redox Biol.* 20, 514–525. doi: 10.1016/j.redox.2018.11.012
- Van der Rest, M. E., Lange, C., and Molenaar, D. (1999). A heat shock following electroporation induces highly efficient transformation of *Corynebacterium glutamicum* with xenogeneic plasmid DNA. *Appl. Microbiol. Biotechnol.* 52, 541–545. doi: 10.1007/s002530051557
- Van Rossum, G., and Drake, F. L. *Python 3 reference manual* CreateSpace: Scotts Valley, CA, (2009).
- Wilks, J. C., and Slonczewski, J. L. (2007). pH of the cytoplasm and periplasm of *Escherichia coli*: rapid measurement by green fluorescent protein fluorimetry. *J. Bacteriol.* 189, 5601–5607. doi: 10.1128/JB.00615-07
- Zeng, W., Guo, L., Xu, S., Chen, J., and Zhou, J. (2020). High-throughput screening Technology in Industrial Biotechnology. *Trends Biotechnol.* 38, 888–906. doi: 10.1016/j.tibtech.2020.01.001